

Entanglement quantification from incomplete measurements: applications using photon-number-resolving weak homodyne detectors

This article has been downloaded from IOPscience. Please scroll down to see the full text article.

2010 New J. Phys. 12 033042

(<http://iopscience.iop.org/1367-2630/12/3/033042>)

View [the table of contents for this issue](#), or go to the [journal homepage](#) for more

Download details:

IP Address: 163.1.203.222

The article was downloaded on 13/05/2010 at 09:49

Please note that [terms and conditions apply](#).

Entanglement quantification from incomplete measurements: applications using photon-number-resolving weak homodyne detectors

Graciana Puentes^{1,7}, Animesh Datta^{2,3}, Alvaro Feito^{2,3}, Jens Eisert^{2,4,5}, Martin B Plenio^{2,3,6} and Ian A Walmsley¹

¹ Clarendon Laboratory, Department of Physics, University of Oxford, OX1 3PU Oxford, UK

² Institute for Mathematical Sciences, Imperial College London, London SW7 2PG, UK

³ QOLS, The Blackett Laboratory, Imperial College London, London SW7 2BW, UK

⁴ Institut für Physik, Universität Potsdam, D-14469 Potsdam, Germany

⁵ Institute for Advanced Study Berlin, D-14193 Berlin, Germany

⁶ Institut für Theoretische Physik, Universität Ulm, D-89069 Ulm, Germany

E-mail: g.puentes1@physics.ox.ac.uk

New Journal of Physics **12** (2010) 033042 (16pp)

Received 12 November 2009

Published 24 March 2010

Online at <http://www.njp.org/>

doi:10.1088/1367-2630/12/3/033042

Abstract. The certificate of success for a number of important quantum information processing protocols, such as entanglement distillation, is based on the difference in the entanglement content of the system quantum states before and after the protocol. In such cases, effective bounds need to be placed on the entanglement of non-local states consistent with statistics obtained from local measurements. In this paper, we study numerically the ability of a hybrid homodyne detector that combines phase sensitivity and photon-number resolution to set accurate bounds on the entanglement content of two-mode quadrature squeezed states without the need for full state tomography. We show that it is possible to set tight lower bounds on the entanglement of a family of two-mode degaussified states using only a few measurements.

⁷ Author to whom any correspondence should be addressed.

This presents a significant improvement over the resource requirements for the experimental demonstration of continuous-variable entanglement distillation, which traditionally relies on full quantum state tomography.

Contents

1. Introduction	2
2. Lower bounds using convex optimization	4
3. Photon-number-resolved weak homodyne detection	5
3.1. Detector model	6
3.2. Unbalanced detection scheme	7
4. Application to continuous-variable entanglement distillation	8
4.1. Two-mode photon-subtracted quadrature squeezed state	9
4.2. Construction of the observables	9
4.3. Numerical results	10
4.4. Tolerance to experimental measurement errors	14
5. Conclusions	15
Acknowledgments	15
References	15

1. Introduction

Entanglement is a fundamental characteristic of quantum systems and a primary resource in quantum information science. Therefore methods to experimentally measure the entanglement of the quantum state of a system are important both for the interpretation of experiments involving quantum systems and for verifying the operation and capacity of a quantum processor or communications system. The most common approach to this problem is to perform quantum tomography of the unknown state of the system. Quantum state tomography amounts to measuring a tomographically complete set of observables, followed by suitably postprocessing the data. For example, in systems specified by continuous variables (such as the quadrature amplitudes of an optical field, or the position and momentum of a mechanical oscillator), the basic theoretical principle is that a collection of probability distributions of the transformed continuous variables is the Radon transform of its Wigner function. Starting from experimentally measured marginals, therefore, an inverse Radon transform gives the Wigner function from which elements of the density matrix can be obtained. The notion was first experimentally realized in the domain of quantum optics [1, 2]. Since then quantum state tomography has been improved to give controlled statistical errors using maximum likelihood [3] or least squares [4], made more efficient for low-rank states using ideas of compressed sensing [5], and equipped with statistical error bars [6]. This is of particular importance in the case of density matrices of non-classical states, which are typically characterized by a negative quasi-probability distribution, such as the Wigner function [7]. Reconstruction of such non-classical states is indeed a part and parcel of experimental demonstrations of quantum information protocols. Non-classical features may be difficult to reconstruct. In photonic applications, this is often due to low quantum detection efficiencies, leading to noisy measurements [8, 9]. Typically, overall detection efficiencies above 50% are

required. However, direct detection of other non-classical signatures may be effected using different sorts of detectors. For example, weak-field homodyne detection coupled with photon counting provides a means to detect entanglement in Gaussian states [10]–[12].

In this work, we present an extensive numerical study of a strategy that provides robust direct quantitative estimates for the entanglement content of a state, without the need for full quantum state tomography [13]. In order to accomplish this task, we systematically investigate the performance of a weak-field homodyne detector with photon-number resolution as an experimentally feasible component for the construction of local measurement operators. These will be a set of positive operator valued measurements (POVMs). The POVM elements required for such a construction are characterized by a model of the homodyne detector, based on a previous characterization of the time-multiplexed photon-number-resolving (PNR) detectors [14]. This detector has also been characterized using the nascent field of detector tomography [15]. The fundamental question we will answer here is the entanglement content of the least entangled state, consistent with the available measurement data [16]–[19]. Thus, we will be left with a *lower* bound on the entanglement of the state in question. In particular, this procedure can be used for setting a lower bound on the logarithmic negativity (LN) [20], the evaluation of which can be reduced to an efficiently solvable class of convex optimization problems called semidefinite programs (SDPs) [16]–[19], [21]. We apply our technique to two mode photon-subtracted quadrature squeezed states. Setting bounds on such a family of non-Gaussian quantum states is of major significance for the implementation of a continuous-variable entanglement distillation protocol [22, 23].

Although we will primarily be concerned with continuous-variable entanglement distillation [23] in this work, we must make it clear at the outset that the technique studied here can be applied to any task that aims to manipulate entanglement between spatially separated observers by local operations and classical communications (LOCCs), and subsequently confirm the outcome, also by means of LOCCs. This goes back to the resource nature of entanglement, and the ability to manipulate it by LOCCs. Continuous variable entanglement distillation is an important instance of such a situation. It should also be clear that we are not limited to entirely optical settings, and similar techniques should be helpful to eventually identify entanglement in opto-mechanical settings, say of entanglement between a micromirror and an optical mode.

In cases such as these, it is often possible to gather enough information by a limited number of measurements to assess the correlations in the state. The natural question then is whether the correlations revealed by these local measurements (aided possibly by classical communication) represent classical correlations, or entanglement [16, 19]. This circumvents the necessity of the resource-intensive process of quantum state tomography. The method is also more robust with respect to measurement errors than full state tomography. Importantly, no *a priori* assumptions concerning the purity or the specific form of the states enter the certifiable bound on the degree of entanglement.

The paper is structured as follows. In section 2, we formalize as an SDP the problem of putting lower bounds on the entanglement content of states using localized measurement statistics. Section 3 describes the specific time-multiplexed homodyne detector that we use to build these localized measurements. In section 4, we present the numerical results on the bounds set on the entanglement content of a two-mode photon subtracted quadrature squeezed state, for different values of relevant experimental parameters. We also present an extensive numerical exploration of the performance of the detector under different experimental conditions. In

particular, we analyse the required phase accuracy and phase stability in our homodyne scheme. We also discuss the tolerance of the convex optimization algorithm to experimental noise. Finally, in section 5, we report the conclusions. As a matter of notation, all logarithms in this paper are taken to base 2.

2. Lower bounds using convex optimization

As stated in the Introduction, we are seeking the amount of entanglement in the least entangled state compatible with a set of measurement results. Mathematically, this can be presented as

$$E_{\min} = \min_{\rho} \{E(\rho) : \text{Tr}(\rho M_i) = m_i\}, \quad (1)$$

where E is the measure of entanglement and M_i are the measurements made with measurement data m_i . Additional constraints that ρ is a density matrix, i.e. positive-definite, and $\text{Tr}(\rho) = 1$ are also imposed. The latter is easily done by setting $M_0 = \mathbb{I}$ and $m_0 = 1$. Depending on the measure of entanglement, and the measurements chosen, the minimization in equation (1) can even be performed analytically, but generically that is not the case. Here, we briefly present a technique following the presentation in [16, 17] that allows the above problem to be cast as an SDP when the entanglement measure is the LN [20].

LN is defined as the logarithm of the 1-norm of the partial transposed density matrix $\|\rho^{T_1}\|_1$. The 1-norm can be expressed as [24]

$$\|\rho^{T_1}\|_1 = \max_{\|H\|_{\infty}=1} \text{Tr}(H\rho^{T_1}) = \max_{\|H\|_{\infty}=1} \text{Tr}(H^{T_1}\rho), \quad (2)$$

with the maximization being over all Hermitian operators H , where $\|\cdot\|_{\infty}$ denotes the standard matrix operator norm, namely the largest singular value of the matrix. Using the monotonicity of the logarithm, the minimization in equation (1) can be rewritten as

$$\mathcal{N}_{\min} = \log \min_{\rho} \left\{ \max_H \{ \text{Tr}(H^{T_1}\rho) : \|H\|_{\infty} = 1 \} : \text{Tr}(\rho M_i) = m_i \right\}. \quad (3)$$

The minimax equality allows us to interchange the maximization and the minimization, leading to

$$\mathcal{N}_{\min} = \log \max_H \left\{ \min_{\rho} \{ \text{Tr}(H^{T_1}\rho) : \text{Tr}(\rho M_i) = m_i \} : \|H\|_{\infty} = 1 \right\}. \quad (4)$$

For any real numbers $\{v_i\}$ for which

$$H^{T_1} \geq \sum_i v_i M_i, \quad (5)$$

clearly the lower bound

$$\text{Tr}(H^{T_1}\rho) \geq \sum_i v_i \text{Tr}(M_i\rho) = \sum_i v_i m_i \quad (6)$$

holds true for states ρ .

Thus we obtain

$$\mathcal{N}_{\min} \geq \log \max_H \left\{ \min_{v_i} \left\{ \sum_i v_i m_i : H^{T_1} \geq \sum_i v_i M_i \right\} : \|H\|_{\infty} = 1 \right\}. \quad (7)$$

Note that the state ρ drops completely out of contention now. Since the inner minimization in equation (4) is an SDP, strong duality in the strictly feasible case ensures equality in equation (7). Thus, having fixed the operators (M_i) that we choose to measure, any choice of H and v_i such that $H^{T_1} \geq \sum_i v_i M_i$ and $\|H\|_\infty = 1$ provides us with a lower bound on the LN of states, which provide expectation values of m_i . Finally, we can rewrite equation (7) as

$$\begin{aligned} & \text{maximize} \quad \log \left(\sum_i v_i m_i \right), \\ & \text{subject to} \quad H^{T_1} \geq \sum_i v_i M_i, \\ & \quad \text{and} \quad -\mathbb{I} \leq H \leq \mathbb{I}, \end{aligned} \tag{8}$$

which can be solved quite easily using standard SDP solvers, like SeDuMi [25], once we have decided what our measurements M_i are. Since these are to be local, the typical form of the measurement, in the case of bipartite states, is

$$M_i = \Pi_j^1 \otimes \Pi_k^2. \tag{9}$$

The problem is thus reduced to the construction of the operators $\Pi_j^{1,2}$, which is what we move onto in the next section. In passing, we mention that the choice of these measurement operators can also be cast as an SDP, although it is more challenging to incorporate the locality constraint into its framework.

This idea gives useful and practically tight bounds to the entanglement content, not having to assume any *a priori* knowledge about the state, or properties of it such as its purity. If the set of expectation values $\{\text{Tr}(M_i \rho)\}$ is tomographically complete, obviously, the bound is promised to give the exact value, but in practice, a much smaller number of measurements is sufficient to arrive at good bounds. Data of expectation values can be composed; that is, if two sets of expectation values are combined, the resulting bound can only become better, to the extent that two sets that only give rise to trivial bounds can provide tight bounds. The approach presented here is perfectly suitable for any finite-dimensional system, and also for continuous-variable systems, as long as the observables M_i are bounded operators. Photon counting with a phase reference gives rise to such operators, as we will see. Note also that similar ideas, formulating lower bounds to entanglement measures, constraining the expectation values of observables can also be formulated for other measures of entanglement [17, 18].

3. Photon-number-resolved weak homodyne detection

We consider now the application of entanglement quantification to the detection of entangled photonic states. In this application we propose to make use of PNR detectors. These have several useful features that make them well suited to the measurement of non-classical signatures of light beams. Firstly, weak-field homodyne detection provides a way to demonstrate the entangled character of EPR-like two-mode squeezed states [10, 11, 26], in contrast to strong-field homodyne detection [27]. Secondly, because the amplitude of the local oscillator (LO) is comparable to that of the signal, the phase sensitivity of the photon counting distribution is much smaller than that of a regular homodyne detector. This greatly reduces the problem of synchronizing local reference frames, which generally becomes more difficult with increasing distance.

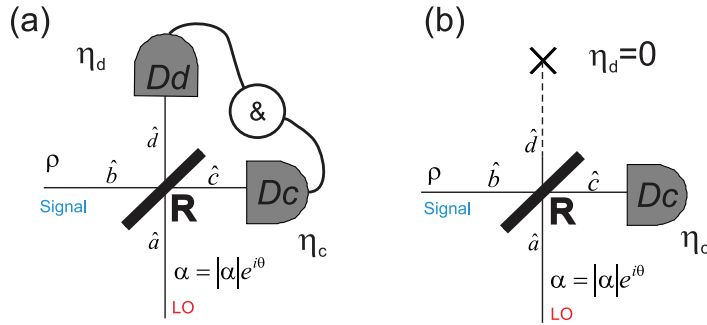


Figure 1. Homodyne detection scheme for (a) balanced and (b) unbalanced configuration. $D_{c,d}$ are PNR detectors of the time-multiplexed type.

Within the framework of the quantum theory of measurement, the action of a detector is completely specified by its POVM set [28]. A POVM element is a positive-definite operator $\Pi_{\beta,\gamma} \geq 0$, which represents the outcome β of a given detector, for a setting γ corresponding to a particular value for a tunable parameter in the detector. In the case of a homodyne detector, γ would correspond to the phase or the amplitude of the LO. The complete set should satisfy $\sum_{\beta} \Pi_{\beta,\gamma} = \mathbb{I}$. The probability $p_{\beta,\gamma}$ of obtaining outcome β for setting γ can be related to the state of the system ρ by $p_{\beta,\gamma} = \text{Tr}(\rho \Pi_{\beta,\gamma})$.

Our detection scheme consists of a weak LO mixed with the signal ρ at a variable reflectivity (R) beamsplitter (BS). The outcome of such an interference is collected by time-multiplexed PNR detectors [29]. The time-multiplexed detectors (TMDs) split the incoming pulses into eight distinct modes by means of a fibre network and a series of 50/50 BSs. These modes are eventually detected by binary avalanche photodetectors (APDs), which can register either 0 or 1 click. Thus there are nine possible outcomes for a given TMD, which are labelled by the number of clicks $\beta = 0, \dots, 8$. The settings of the detector γ , in turn, are determined by a number of experimental parameters, such as LO amplitude $|\alpha|$ and phase θ , BS reflectivity R , and detector efficiency η . By tuning the detector settings it is possible to prepare POVM elements able to project onto a large variety of radiation field states, ranging from Fock states to quadrature squeezed states [14].

3.1. Detector model

In figure 1(a), we show a schematic of our detection system for the balanced configuration. The BS input modes, labelled ‘a’ and ‘b’, correspond to the LO and the signal (ρ), respectively. The output modes, labelled by ‘c’ and ‘d’, are detected by PNR detectors D_c and D_d . The joint detection events, denoted $\{\beta = (n_c, n_d)\}$, are recorded for different LO settings $\gamma = (|\alpha|, \theta)$. The LO is prepared in a coherent state with state vector $|\alpha\rangle$ of complex amplitude $\alpha = |\alpha|e^{i\theta}$ and provides the phase reference needed to access off-diagonal elements in ρ , as the PNR detectors alone have no phase sensitivity [29]. For ideal PNR detectors, the probability to obtain measurement outcome β for LO setting γ is related to ρ by [30]

$$p_{\beta,\gamma} = \text{Tr}_{c,d}[U \sigma U^\dagger |n_c, n_d\rangle \langle n_c, n_d|], \quad (10)$$

where $U = e^{i\chi(b^\dagger a + a^\dagger b)}$ is the unitary operator representing the BS, $R = \cos(\chi)^2$ is the BS reflectivity, $\sigma = |\alpha\rangle \langle \alpha|_a \otimes \rho_b$ the two-mode input state and $|n_c, n_d\rangle = |n_c\rangle_c |n_d\rangle_d$ the photon number state vectors of mode c (d) to be detected at PNR detectors D_c (D_d).

In order to account for the imperfections of the time-multiplexed PNR detectors, we use a well-tested model of the TMDs [29]. Within this model, the TMD operation can be described as a map from the incoming photon-number distribution \vec{r} , as a vector (i.e. the diagonal components of the density matrix), to the measured click statistics \vec{k} by $\vec{k} = C \cdot L \cdot \vec{r}$. Here L and C are matrices accounting for loss and the intrinsic detector structure [29], respectively. To calculate the POVM elements implemented by our PNR homodyne detector, the POVMs for TMD detectors D_c and D_d are determined from the C and L matrices (characterized by independent methods [15]). The TMD POVMs are then substituted into equation (10), in place of the photon number projectors $|n_c, n_d\rangle\langle n_c, n_d|$, to obtain the final expression for the imperfect POVM elements $\Pi_{\beta,\gamma}$. We note that our TMDs can resolve up to eight photons, setting the number of possible outcomes to 81. The TMDs described here can be dealt with in a rather general way. In this work, a particular choice of splitting ratios was made for simplicity, but a full model of the detector is also available [29].

3.2. Unbalanced detection scheme

Our aim is to use such homodyne PNR detectors to provide lower bounds on the entanglement of bipartite quantum states, in which case two of such devices should be employed. To this end, the joint POVM statistics of the four modes involved in the detection need to be measured, increasing the total number of POVM elements to $81^2 = 6561$. In order to simplify the experimental arrangement, we use the detector in an unbalanced configuration, so that we detect only one of the outgoing modes of each homodyne BS. In this way only two modes need to be jointly detected and the total number of POVM elements is reduced to $9^2 = 81$. This unbalanced scheme can be modelled by setting the efficiency η of one of the PNR detectors to zero (see figure 1(b)). The only disadvantage of this unbalanced scheme is that the overall efficiency is in principle reduced by 50%, but this limitation can be overcome by increasing the BS reflectivity R . Additionally, as we will show in the next section, our partial detection approach alleviates the strong efficiency requirements of full tomography, allowing for additional losses of the unbalanced scheme.

In figure 2, we show numerically constructed Wigner functions corresponding to six different POVM elements $\Pi_{\beta,\gamma}$, characterizing the unbalanced scheme. The axes (x, p) label the phase space quadratures. The different columns correspond to different LO phases $\theta = 0$ and $\theta = \pi/2$. The rows correspond to three consecutive outcomes $\beta = 1, 2$ and 3 labelling the corresponding number of detector clicks. For these simulations we fixed the amplitude of the LO to $|\alpha| = 1$, the BS reflectivity to $R = 50\%$ and the detector efficiency to $\eta = 10\%$, which is a realistic value for a single mode TMD. The figure shows that $\Pi_{\beta,\gamma}$ are not rotationally symmetric, as expected for a phase-sensitive detector. The oscillations in the Wigner functions are due to the low efficiency of the detectors, which mixes different photon number states, whose phase-space representation is given by consecutive rings of increasing radii. Also, as is expected, a change in the LO phase setting by $\pi/2$ corresponds to an overall phase-space rotation in the Wigner function. In the next section we show that by using eight POVM elements of the type shown in figure 2 for each subsystem, we can construct the measurements M_i mentioned in section 2, which can be employed to bound the entanglement content of two-mode degaussified states.

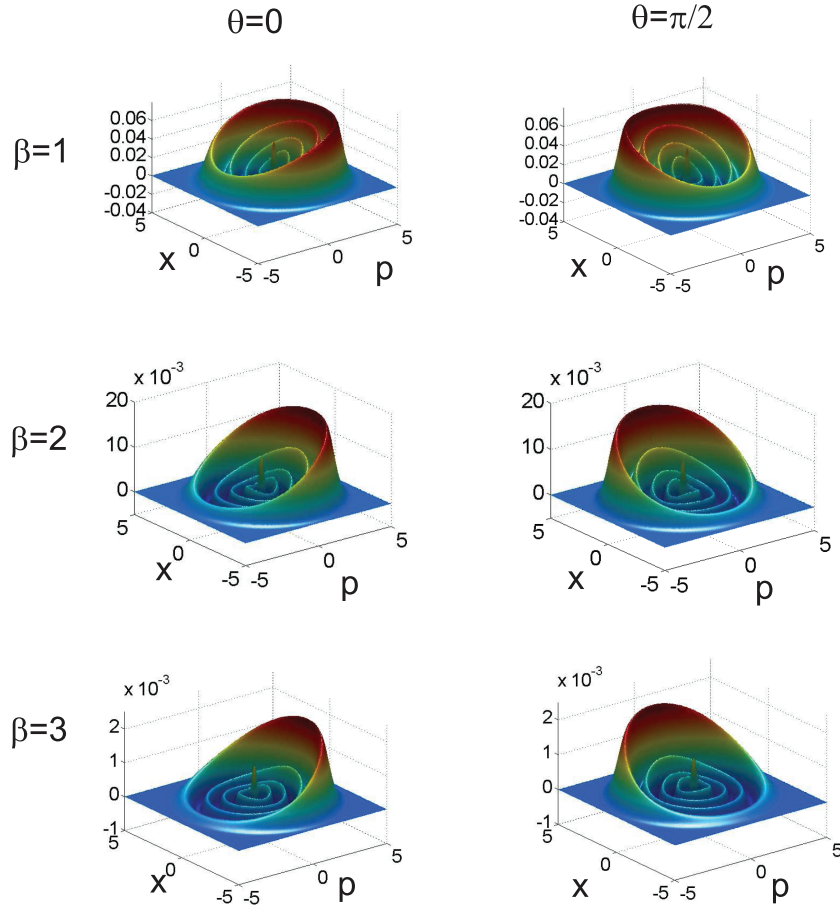


Figure 2. Wigner representation of selected POVM elements $\Pi_{\beta,\gamma}$ for the unbalanced scheme described in figure 1(b). Different columns correspond to LO phase settings $\theta = 0$ and $\theta = \pi/2$. The rows correspond to three different detector outcomes $\beta = 1, 2, 3$. The amplitude of the LO, BS reflectivity and detector efficiency are $|\alpha| = 1$, $R = 50\%$ and $\eta = 10\%$, respectively.

4. Application to continuous-variable entanglement distillation

We will now apply the above methods to a setting that plays a central role in continuous-variable entanglement distillation. Entanglement distillation aims at producing more highly entangled states out of a situation where entanglement is present only in a dilute and noisy form, presumably generated by some lossy quantum channel. It provides the key step in quantum repeater ideas allowing for the distribution of long-range entanglement in the presence of noise. Crudely speaking, one may distinguish between actual distillation schemes that involve more than one specimen of an entangled state at each step of the protocol and ‘Procrustean’ or local filtering approaches that take a single copy of a state and, under appropriate local filtering, give rise—if successful—to a more highly entangled state. In the setting of strict Gaussian operations, continuous-variable entanglement distillation of neither kind is possible [23], but this obstacle can be overcome with the help of non-Gaussian ingredients such as photon addition or subtraction [22]. Such first Procrustean steps can also be used as starting points in full

entanglement distillation protocols. Indeed, quite exciting first steps towards full continuous-variable entanglement distillation have recently been taken experimentally [9], [32]–[35].

In a subsequent discussion, we show the use of quantitative tests to certify success in such a scheme. Needless to say, we discuss specific input states, but it should be clear that the given entanglement bounds do not make use of that *a priori* knowledge. We consider as our initial state vector $|\psi^{\text{ini}}\rangle$ an ideal pure two-mode quadrature squeezed state of the form

$$|\psi^{\text{ini}}\rangle = \sqrt{1 - \lambda^2} \sum_{n=0}^{\infty} \lambda^n |n, n\rangle_{1,2}, \quad (11)$$

where λ represents the squeezing parameter, and the subindices (1,2) represent each spatial mode. Such a type of states is produced in the laboratory by the nonlinear process of spontaneous parametric down conversion (SPDC) in nonlinear crystals [31]. In order to simplify our numerical calculations, we will restrict the maximum photon number per mode to $n_{\text{max}} = 3$. Thus the set of bipartite initial states $\rho_{1,2}^{\text{ini}}$ is given by the set of 16×16 density matrices $\rho_{1,2}^{\text{ini}} = |\psi^{\text{ini}}\rangle\langle\psi^{\text{ini}}|$. The LN for the bipartite state in equation (11) takes the simple form

$$\mathcal{N}(\rho_{1,2}^{\text{ini}}) = \log \|(\rho_{1,2}^{\text{ini}})^{T_1}\|_1 = \log \left(\frac{1 + \lambda}{1 - \lambda} \right), \quad (12)$$

as can readily be verified.

4.1. Two-mode photon-subtracted quadrature squeezed state

In order to distill continuous-variable entanglement from Gaussian states, such as the two-mode quadrature squeezed state described by equation (11), an operation that removes the Gaussian nature of the probability distribution is required [22]. Examples of such non-Gaussian operations include the conditional subtraction or addition of a photon [9, 35]. An ideal two-mode photon-subtracted quadrature squeezed state can be modelled by inserting a BS of transmission T (the so-called subtraction BS (SBS)) in one spatial mode. The reflected mode from the SBS is then detected by a standard avalanche photodetector (APD) (this is schematized in figure 3). The photon subtracted state can, in the approximation of having a very weakly reflecting BS, thus be written as

$$|\psi^{\text{subt}}\rangle = C \sum_{n=1}^{n_{\text{max}}} (\lambda T)^n \sqrt{n} |n-1, n\rangle_{1,2}, \quad (13)$$

where C is a normalization constant and in our simulations $n_{\text{max}} = 3$. The corresponding density matrix is $\rho_{1,2}^{\text{subt}} = |\psi^{\text{subt}}\rangle\langle\psi^{\text{subt}}|$. We note that the family of states described by equation (13) are of current interest in the realm of continuous-variable entanglement distillation, as they represent a particular kind of non-Gaussian state (i.e. a state whose Wigner representation is not Gaussian), whose entanglement content $\mathcal{N}(\rho_{1,2}^{\text{subt}})$ is predicted to be larger than $\mathcal{N}(\rho_{1,2}^{\text{ini}})$, for suitable experimental parameters (λ, T) [23].

4.2. Construction of the observables

Our aim is to construct bipartite measurement operators M_i as a tensor product of the POVM elements corresponding to each subsystem $\Pi_1 \otimes \Pi_2$. In particular, we will consider eight POVM elements for each subsystem (1, 2), specified by four different outcomes $\beta = 0, 1, 2, 3$ and two

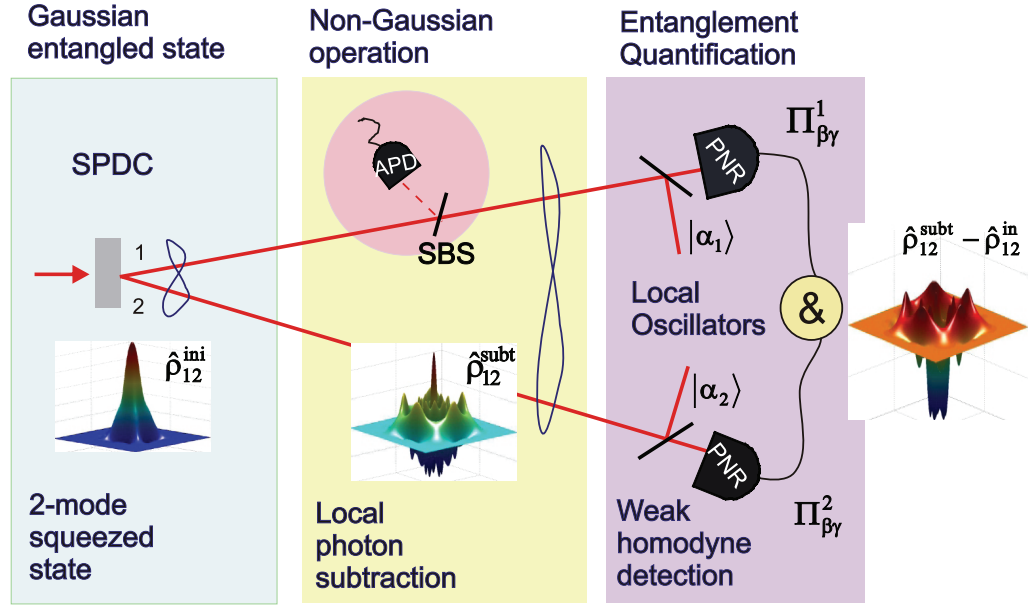


Figure 3. Scheme describing the bipartite initial state $\rho_{1,2}^{ini}$ produced by SPDC. Next, the photon-subtracted state $\rho_{1,2}^{subt}$ is prepared by local subtraction of a single photon at a tunable SBS. The entanglement content in $\rho_{1,2}^{subt}$ is quantified by our partial detection approach. This type of scheme is one of the main components of an entanglement distillation protocol [22].

different settings γ corresponding to $\theta = 0$ and $\theta = \pi/2$. Thus the selected POVM subset for each mode consists of eight elements $\Pi_{\beta,\gamma}$, collected as

$$\{\Pi_{0,0}, \Pi_{1,0}, \Pi_{2,0}, \Pi_{3,0}, \Pi_{0,\pi/2}, \Pi_{1,\pi/2}, \Pi_{2,\pi/2}, \Pi_{3,\pi/2}\}, \quad (14)$$

where we will keep this ordering in the POVM elements for the rest of the paper. We measure 8×8 configurations, which determine 64 POVMs M_i , labelled by the index i , of the form in equation (9) with $j, k = 1, \dots, 8$ being the indices labelling the POVM elements of mode (1, 2) respectively, and $i = (j, k)$ the joint index, labelling the bipartite measurement operator. For example, the observable $M_{(6,1)}$ corresponds to the POVM elements $\Pi_{1,\pi/2}$ for mode 1 and $\Pi_{0,0}$ for mode 2. This gives a total of 64 measurements, which in turn determine 64 expectation values $\text{Tr}(\rho_{1,2} M_i) = m_i$, with $i = 1, \dots, 64$. This is a clear reduction with respect to full state tomography, which would require (at least) $16^2 - 1 = 255$ measurements in order to reconstruct $\rho_{1,2}$ in a truncated Hilbert space of dimension 16.

In order to find the lower bound on the LN of the photon-subtracted states $\rho_{1,2}^{subt}$ described in equation (13), by means of the set of measurement observables M_i as defined in equation (9), we follow the procedure described in section 2. Note that in a real experiment $\text{Tr}(\rho_{1,2}^{subt} M_i)$ should be replaced by the actual experimental probability estimates, which will be subject to different sources of noise. We will discuss the effect of experimental noise on entanglement bounds in the final subsection.

4.3. Numerical results

Figure 4 presents the percentual entanglement increase between $|\psi^{ini}\rangle$ (red curve) and $|\psi^{subt}\rangle$ (blue curve) for different squeezing parameters λ ranging from $\lambda = 0.1$ to $\lambda = 0.3$. Percentual

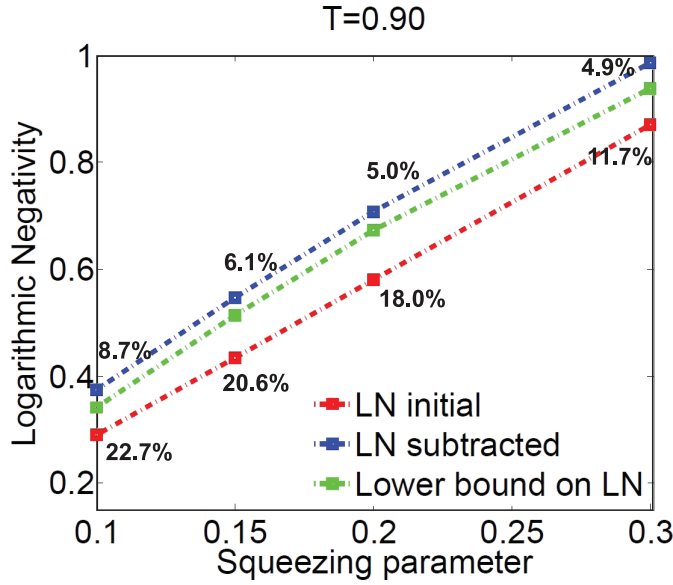


Figure 4. LN for the initial state (red curve), subtracted state (blue curve) and lower bound on LN of the subtracted state obtained by convex optimization (green curve) versus the squeezing parameter (λ). Percentual entanglement increase with a single photon-subtraction step and percentual difference between the actual LN of the subtracted state and the one obtained by convex optimization are indicated. The SBS transmission was fixed at $T = 90\%$.

differences between the actual LN characterizing the photon-subtracted state and the lower bound obtained by convex optimization (green curve) are also indicated. The transmission coefficient of the SBS in figure 2 was fixed at ($T = 90\%$); the LO amplitude and detector efficiency were set to $|\alpha| = 1$ and $\eta = 10\%$, respectively. It is noticeable that while a single-photon-subtraction step produces a larger entanglement increase for lower values of λ , the lower bound on the entanglement becomes tighter for higher squeezing parameter λ . The percentual error in the lower bound is in all cases below 9%, which reveals the accuracy of our partial detection scheme in characterizing entanglement.

Figure 5 presents the percentual entanglement increase between $|\psi^{\text{ini}}\rangle$ (red curve) and $|\psi^{\text{subt}}\rangle$ (blue curve) for different SBS transmissions T , ranging from $T = 80\%$ to 99% . Percentual differences between the actual LN characterizing the photon-subtracted state vector ($|\psi^{\text{subt}}\rangle$) and the lower bound obtained by convex optimization (green curve) are also indicated. The squeezing parameter was fixed at ($\lambda = 0.2$) and the LO amplitude and detector efficiency were set to $|\alpha| = 1$ and $\eta = 10\%$, respectively. Figure 5 shows that for a fixed squeezing parameter the single-photon-subtraction step produces a larger entanglement increase for higher SBS transmission T and that the lower bound becomes tighter for higher T . In all cases, the percentual error in the lower bound remains below 11%.

Next, we tested the robustness of the measurement scheme with respect to different types of LO phase noise. To this end, we constructed a set of 64 POVM elements as described in the previous section, for a fixed LO amplitude $|\alpha| = 1$, detector efficiency $\eta = 0.10$, SBS transmission $T = 0.90$ and squeezing parameter $\lambda = 0.2$. The two fixed phase settings $\theta_0 = (0, \pi/2)$ were subject to different types of fluctuations. In particular, we investigated the

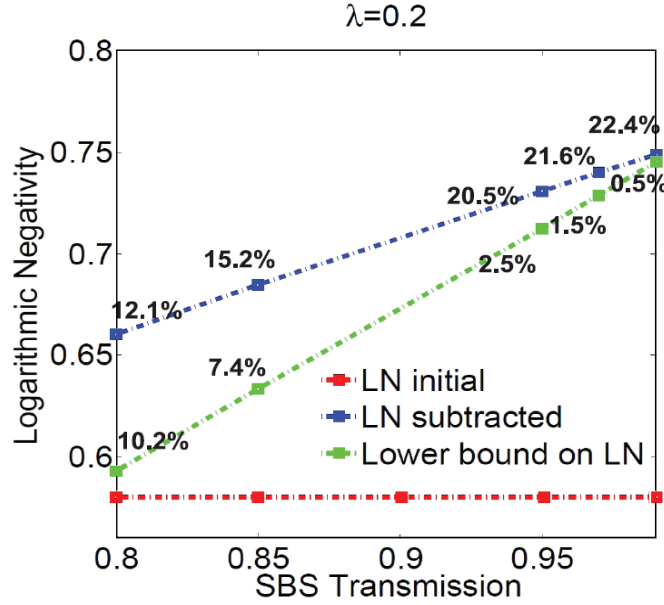


Figure 5. LN for the initial state (red curve), subtracted state (blue curve) and lower bound on LN of the subtracted state obtained by convex optimization (green curve), versus SBS transmission (T). Percentual entanglement increase with a single photon-subtraction step and percentual difference between the actual LN of the subtracted state and the one obtained by convex optimization are indicated. The squeezing parameter was fixed at $\lambda = 0.2$.

required precision in the LO phase θ by adding different amounts of random phase noise ϵ in the form $\theta = (0 \pm \epsilon/10, \pi/2(1 \pm \epsilon/10))$, where $0 \leq \epsilon \leq 1$ is a random number with a uniform distribution. In our numerical simulations we found that for a phase error of up to 10%, the lower bound differs from the actual LN by less than 1%. This means that an LO phase precision of 5° (at the most) is required for the bounds to produce a highly tight estimate. This is shown in figure 6(a); for $\theta_0 = (0, \pi/2)$, the squeezing parameter $\lambda = 0.2$, the SBS transmission $T = 90\%$, the LO amplitude $|\alpha| = 1$ and the detector efficiency $\eta = 0.10$.

We also analysed the effect of temporal phase fluctuations by modelling the LO as a phase averaged coherent state described by the complex amplitude $\alpha = \sum_j |\alpha| e^{i(\theta_0 + \delta\theta_j)}$ with $j = 1, \dots, 100$ and $\delta\theta$ a random phase with a uniform distribution centred around $\theta_0 \in [0, \pi/2]$ and with width $\Delta\theta$. We found that a phase width of up to 0.6 rad ($\approx 30^\circ$) introduces a percentual difference in the lower bound of up to 15%. For a phase width $\Delta\theta$ of up to 0.4 rad ($\approx 20^\circ$), the lower bound on the LN is within 10%. This is shown in figure 6(b); for the squeezing parameter $\lambda = 0.2$, the SBS transmission $T = 90\%$, the LO amplitude $|\alpha| = 1$ and the detector efficiency $\eta = 0.10$.

Finally, we analysed the impact of a different homodyne BS reflectivity R on the overall accuracy of the entanglement quantification scheme. We found that for $R \geq 80\%$ the lower bound on the LN differs by less than 0.2% from the actual value, as long as the LO amplitude remains small enough ($|\alpha| \leq 2.5$) owing to the limited photon-number resolution in the TMDs. This is shown in figure 7(a). Figure 7(b) shows a complete simulation for $50\% \leq R \leq 99\%$, $|\alpha| = 2.5$, $\lambda = 0.1$ and $T = 90\%$. In all the simulations, the TMD efficiencies were set to

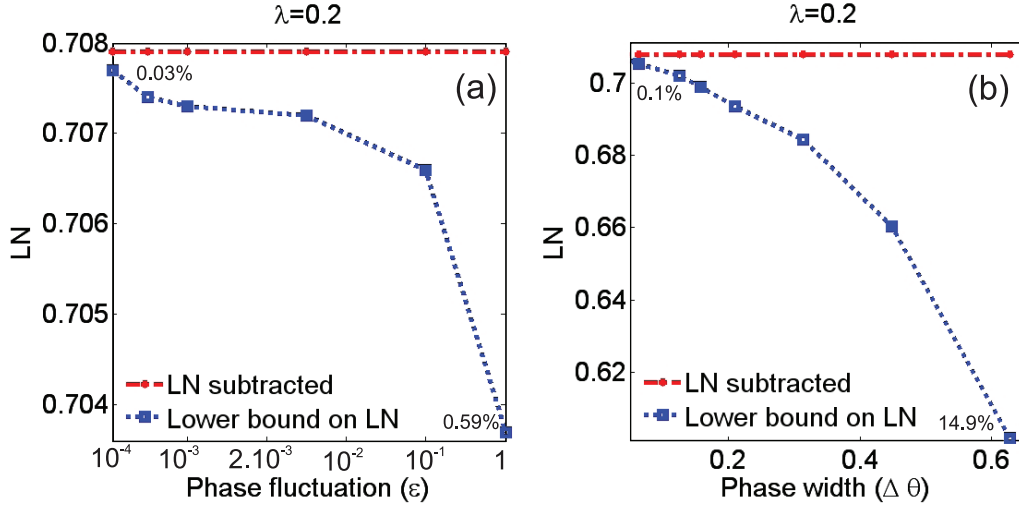


Figure 6. Exact LN (red curve) and lower bound obtained by convex optimization (blue curve) for the photon-subtracted state versus (a) dimensionless phase noise ϵ and (b) phase noise standard deviation $\Delta\theta$ in radians for LO phase settings $\theta_0 = (0, \pi/2)$. Maximum and minimum percentual differences are indicated. The squeezing parameter was fixed at $\lambda = 0.2$.

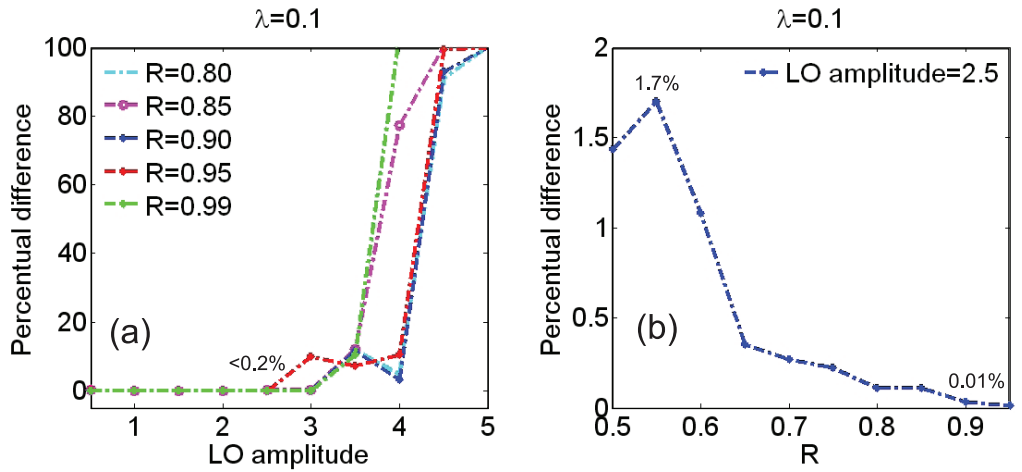


Figure 7. (a) Percentual error in the lower bound set by convex optimization for different homodyne BS reflectivities R . The error remains below 0.2% for a sufficiently weak LO amplitude $|\alpha| < 2.5$. (b) Extension to a larger range of BS reflectivities R , for $\lambda = 0.1$, $|\alpha| = 2.5$ and $\theta = (0, \pi/2)$.

$\eta = 0.10$ and the LO phase settings were chosen as $\theta = (0, \pi/2)$. Additionally, the subtraction APD in figure 3 is assumed to have a limited efficiency, which is modelled by interposing a BS with a transmittivity of 15% ⁸.

⁸ All the simulations in this work were performed using the convex optimization routine SeDuMi 1.1 (see [25]).

4.4. Tolerance to experimental measurement errors

In the numerical simulations presented here, we have used the exact expectation values $m_i = \text{Tr}(\rho^{\text{subt}} M_i)$ for the minimization of LN. However, in a real experiment, such expectation values are affected by different sources of noise. In this subsection, we test the tolerance of the scheme to experimental errors. There are several ways to include such an error. One approach would be to estimate variances of measured values and then make a model including Gaussian-distributed errors for the measured variables. Another would be a hard bound on the degree of entanglement as a function of a small norm deviation from the perfect data, giving rise to a box error model. This latter error model even allows for a malicious correlation in the errors, in that all errors add constructively. Clearly, independent, identically distributed errors would give rise to much more robust bounds.

Nonetheless, in order to evaluate the feasible robustness of our method, we will now refer to this latter, more demanding error model: we merely require for $\epsilon > 0$ that the measured value n_i and the true expectation value $m_i = \text{Tr}(M_i \rho)$ satisfy $m_i \in [(1 - \epsilon)n_i, (1 + \epsilon)n_i]$ for all i . Hence, the problem to be solved becomes

$$\mathcal{N}_{\min} = \min_{\rho} \{ \mathcal{N}(\rho) : \text{Tr}(\rho M_i) = n_i, m_i \in [(1 - \epsilon)n_i, (1 + \epsilon)n_i] \ \forall i \}. \quad (15)$$

Including such measurement errors, equation (8) then clearly becomes

$$\begin{aligned} & \text{maximize} \quad \log \left(\sum_i v_i n_i \right), \\ & \text{subject to} \quad H^{T_1} \geq \sum_i v_i M_i, \\ & \quad m_i \in [(1 - \epsilon)n_i, (1 + \epsilon)n_i] \ \forall i, \\ & \quad \text{and} \quad -\mathbb{I} \leq H \leq \mathbb{I}, \end{aligned} \quad (16)$$

which can be solved as easily as equation (8) using SeDuMi [25]. Note that the resulting bound is even valid if each of the errors in the measured data is maliciously correlated.

In this subsection, we use as an example a two-mode squeezed state with $\lambda = 0.2$ from which a photon is subtracted using an SBS with $T = 95\%$. The APD in figure 2 is assumed to have a limited efficiency, which is achieved by interposing a BS with a transmittivity of 20%. In the short table below, we present the bounds attained by solving the SDP in equation (16) for a range of values of ϵ , corresponding to realistic experimental noise levels [31].

ϵ	0.0	0.001	0.01	0.1
\mathcal{N}_{\min}	0.7308	0.7185	0.6660	0.3034

These numbers must be compared with the entanglement of the initial two-mode squeezed state, which has $\mathcal{N} = 0.5803$, and the ideal photon subtracted state, which has $\mathcal{N} = 0.7309$. Note that the state on which we put the lower bounds is inevitably mixed, and the table shows the robustness and effectiveness of our scheme. $\epsilon = 0.01$ is enough to demonstrate the enhancement of entanglement by distillation with experimentally realistic parameters, without having to undertake a full tomographic reconstruction of the quantum states involved. This value of ϵ translates to about 10000 data points, via the central limit theorem, for each measurement configuration. This is in line with the number of data points taken in other experiments involving reconstruction of non-Gaussian states [9].

5. Conclusions

We have presented quantitative numerical evidence that a novel homodyne detection scheme with photon-number resolution is able to set accurate bounds on the entanglement content of a family of two-mode photon-subtracted quadrature squeezed states. The entanglement lower bounds retrieved by the measurement scheme are accurate to within 10% for the full range of squeezing parameters $\lambda = 0.1$ – 0.3 and SBS transmissions $T = 80\%$ – 99% . We found that the bounds become tighter for higher λ and T . We also analysed the required phase precision and stability in the LO and found that a precision of less than 5° is required for a bound accuracy within 1%, while temporal phase fluctuations of up to 20° can be accepted for a lower bound with 10% accuracy. Additionally we found that a homodyne SBS reflectivity R above 60%, for an LO amplitude within $|\alpha| = 2.5$ is sufficient to obtain a lower bound on the LN, which agrees to within 2% with the actual LN value characterizing the photon-subtracted state. The results reported here provide strong numerical evidence of the suitability of our partial detection scheme for entanglement quantification of bipartite degaussified states. We note that this type of partial detection approach is attractive not only due to its accuracy but also due to its scalability. This is of importance for the application of an entanglement distillation protocol combining two degaussified sources [22, 23]. In particular, our scheme can be easily scaled to the detection of four spatial modes, in which case it would require the measurement of only $64^2 = 4096$ outcome probabilities. In contrast, full state tomography would require (at least) $16^4 - 1 = 65\,535$ different measurements. Therefore our method provides a feasible, direct and resilient way of accurately experimentally characterizing entanglement in continuous-variable quantum systems. Finally, we anticipate the amount of data required in order to obtain an adequate precision in the measurement-outcome probabilities characterizing our partial measurement scheme to be considerably lower than that required for full state tomography.

Acknowledgments

This work was supported by the EPSRC through the QIP IRC and by the EU through the IST directorate FET Integrated Project QAP and through STREP projects CORNER, HIP, COMPAS and MINOS. JE acknowledges support through a EURYI Award, MP and IAW through Royal Society Research Merit Awards and MP through an Alexander von Humboldt Professorship.

References

- [1] Smithey D, Beck M, Raymer M and Faridani A 1993 *Phys. Rev. Lett.* **70** 1244
- [2] Dunn T, Walmsley I A and Mukamel S 1995 *Phys. Rev. Lett.* **74** 884
- [3] Hradil Z 1997 *Phys. Rev. A* **55** R1561
- [4] Branderhorst M P A, Walmsley I A, Kosut R L and Rabitz H 2008 *J. Phys. B* **41** 074004
Kosut R L, Walmsley I A and Rabitz H 2004 arXiv:quant-ph/0411093
- [5] Kosut R L 2008 arXiv:0812.4323
Gross D, Liu Y-K, Flammia S, Becker S and Eisert J 2009 arXiv:0909.3304
Shabani A, Kosut R L and Rabitz H 2009 arXiv:0910.5498
- [6] Audenaert K M R and Scheel S 2009 *New J. Phys.* **11** 023028
- [7] Hillery M, O'Connell R F, Scully M O and Wigner E P 1984 *Phys. Rep.* **106** 121
Schleich W P 2001 *Quantum Optics in Phase Space* (Berlin: Wiley)
- [8] Lvovsky A I and Raymer M G 2009 *Rev. Mod. Phys.* **81** 299

- [9] Ourjoumtsev A, Dantan A, Tualle-Brouiri R and Grangier P 2007 *Phys. Rev. Lett.* **98** 030502
- [10] Grangier P, Potasek M J and Yurke B 1988 *Phys. Rev. A* **38** R3132
- [11] Kuzmich A, Walmsley I A and Mandel L 2000 *Phys. Rev. Lett.* **85** 1349
- [12] Wallentowitz S and Vogel W 1996 *Phys. Rev. A* **53** 4528
- [13] Horodecki R, Horodecki M and Horodecki P 1999 *Phys. Rev. A* **59** 1799
- [14] Puentes G, Lundeen S J, Branderhorst A M P, Coldenstrodt-Ronge H B, Smith B J and Walmsley I A 2009 *Phys. Rev. Lett.* **102** 080404
- [15] Lundeen J S, Feito A, Coldenstrodt-Ronge H, Pregnell K L, Silberhorn Ch, Ralph T C, Eisert J, Plenio M B and Walmsley I A 2009 *Nat. Phys.* **5** 27
Feito A, Lundeen J S, Coldenstrodt-Ronge H, Eisert J, Plenio M B and Walmsley I A 2009 *New J. Phys.* **11** 093038
Coldenstrodt-Ronge H B, Lundeen J S, Feito A, Smith B J, Maurer W, Silberhorn Ch, Eisert J, Plenio M B and Walmsley I A 2009 *J. Mod. Opt.* **56** 432
- [16] Audenaert K M R and Plenio M B 2006 *New J. Phys.* **8** 266
- [17] Eisert J, Brandão F G S L and Audenaert K M R 2007 *New J. Phys.* **9** 46
- [18] Gühne O, Reimpell M and Werner R F 2007 *Phys. Rev. Lett.* **98** 110502
- [19] Plenio M B 2009 *Science* **324** 342
- [20] Plenio M B 2005 *Phys. Rev. Lett.* **95** 090503
Eisert J 2001 *PhD Thesis* Potsdam
Vidal G and Werner R F 2002 *Phys. Rev. A* **65** 032314
- [21] Boyd S and Vandenberghe L 2005 *Convex Optimization* (Cambridge: Cambridge University Press)
- [22] Browne D E, Eisert J, Scheel S and Plenio M B 2003 *Phys. Rev. A* **67** 062320
Eisert J, Browne E D, Scheel S and Plenio B M 2004 *Ann. Phys. (NY)* **311** 431
- [23] Eisert J, Scheel S and Plenio B M 2002 *Phys. Rev. Lett.* **89** 137903
Fiurasek J 2002 *Phys. Rev. Lett.* **89** 137904
Giedke G and Cirac I J 2002 *Phys. Rev. A* **66** 032316
- [24] Bhatia R 1997 *Matrix Analysis* (New York: Springer)
- [25] Available for free downloading at <http://sedumi.ie.lehigh.edu>
- [26] Banaszek K and Wodkiewicz K 1998 *Phys. Rev. A* **58** 4345
Banaszek K and Wodkiewicz K 1999 *Phys. Rev. Lett.* **82** 2009
- [27] Ou Z Y, Pereira S F, Kimble H J and Peng K C 1992 *Phys. Rev. Lett.* **68** 3663
- [28] Holevo A S 1982 *Probabilistic and Statistical Aspects of Quantum Theory* (Amsterdam: North-Holland)
- [29] Achilles D, Silberhorn C, Sliwa C, Banaszek K, Walmsley I A, Fitch M J, Jacobs B C, Pittman T D and Franson J D 2004 *J. Mod. Opt.* **51** 1499
- [30] Pregnell K L and Pegg D T 2002 *Phys. Rev. A* **66** 013810
- [31] Mosley J P, Lundeen S J, Smith J B, Wasylczyk P, U'Ren A B, Silberhorn Ch and Walmsley A I 2008 *Phys. Rev. Lett.* **100** 133601
- [32] Dong R, Lassen M, Heersink J, Marquardt Ch, Filip R, Leuchs G and Andersen U 2008 *Nat. Phys.* **4** 919
Hage B, Samblowski A, DiGuglielmo J, Franzen A, Fiurasek J and Schnabel R 2008 *Nat. Phys.* **4** 915
- [33] Takahashi H, Neergaard-Nielsen J, Takeuchi M, Takeoka M, Hayasaka K, Furusawa A and Sasaki M 2009 arXiv:0907.2159
- [34] Xiang G Y, Ralph T C, Lund A P, Walk N and Pryde G J 2009 arXiv:0907.3638
- [35] Parigi V, Zavatta A, Kim S M and Bellini M 2007 *Science* **317** 1890